The Midlatitude Response to Polar Sea Ice Loss: Idealized Slab-Ocean Aquaplanet Experiments with Thermodynamic Sea Ice

TIFFANY A. SHAW[a] AND ZOË SMITH[b]

[a] *Department of the Geophysical Sciences, University of Chicago, Chicago, Illinois*
[b] *Department of Physics, University of Chicago, Chicago, Illinois*

(Manuscript received 2 July 2021, in final form 4 January 2022)

ABSTRACT: Slab-ocean aquaplanet simulations with thermodynamic sea ice are used to study the zonally symmetric mechanisms whereby polar sea ice loss impacts the midlatitude atmosphere. Imposed sea ice loss (difference without and with sea ice with historical CO_2 concentration) leads to global warming, polar amplified warming, and a weakening of poleward atmospheric energy transport and the midlatitude storm-track intensity. The simulations confirm an energetic mechanism that predicts a weakening of storm-track intensity in response to sea ice loss, given the change of surface albedo and assuming a passive ocean. Namely, sea ice loss increases the absorption of shortwave radiation by the surface (following the decrease of surface albedo), which increases surface turbulent fluxes into the atmosphere thereby weakening poleward atmospheric energy transport. The storm-track intensity weakens because it dominates poleward energy transport. The quantitative prediction underlying the mechanism captures the weakening but underestimates its amplitude. The weakening is also consistent with weaker mean available potential energy (polar amplified warming) and scales with sea ice extent, which is controlled by the slab-ocean depth. The energetic mechanism also operates in response to sea ice loss due to melting (difference of the response to quadrupled CO_2 with and without sea ice). Finally, the midlatitude response to sea ice loss in the aquaplanet agrees qualitatively with the response in more complex climate models. Namely, the storm-track intensity weakens and the energetic mechanism operates, but the method used to impose sea ice loss in coupled models impacts the surface response.

KEYWORDS: Sea ice; Atmospheric circulation; Energy transport; Storm tracks; Kinetic energy; General circulation models

1. Introduction

Observations show rapid climate change in the Arctic such as declining sea ice cover and warming (Graversen et al. 2008; Screen and Simmonds 2010). While climate models in the 1970s predicted sea ice decline and Arctic amplification (AA) of surface warming in response to a doubling of CO_2 concentration (Manabe and Wetherald 1975), many open questions remain regarding the impact on other regions. A particular region of interest is the midlatitudes (~30°–60° latitude) where the dynamics are dominated by storm tracks and jet streams (Cohen et al. 2014; Barnes and Screen 2015; Overland et al. 2015; Francis 2017; Cohen et al. 2020).

A significant challenge to understanding the mechanisms whereby observed Arctic climate change impacts the midlatitude atmosphere is the low signal-to-noise ratio (Barnes 2013; Blackport and Screen 2020). Consequently, climate model simulations have been used to quantify the signal and understand the underlying mechanisms. State-of-the-art coupled climate model simulations have demonstrated several robust zonally symmetric responses to imposed sea ice loss (response to end-of-the-century sea ice conditions with historical CO_2 concentration). For example, in response to sea ice loss there is global warming, AA of surface warming, tropical warming aloft, weakened poleward atmospheric energy transport, weakening and equatorward shift of the eddy-driven jet, and equatorward shift of the ITCZ (e.g., Deser et al. 2015; Blackport and Kushner 2017; McCusker et al. 2017; England et al. 2018; Screen et al. 2018; England et al. 2020; Audette et al. 2021). However, other zonally asymmetric signals are less robust, for example, the warm Arctic–cold Eurasia surface temperature response (McCusker et al. 2016; Screen et al. 2018). While there are several robust zonally symmetric responses, there are also many open questions regarding the mechanisms and how the method used to impose sea ice loss in coupled models (ghost forcing, albedo, or nudging) impacts the response (Screen et al. 2018; Smith et al. 2019; Sun et al. 2020).

In reality sea ice loss is driven by a forcing, for example, melting due to increased CO_2 concentration. Sea ice melting, increased CO_2, and AA are quantitatively linked in observations and climate models (Screen and Simmonds 2010; Dai et al. 2020; Feldl et al. 2020). However, the connection between the midlatitude response to imposed sea ice loss with historical CO_2 concentration and sea ice loss due to melting induced by increased CO_2 concentration is unclear. In particular, the different CO_2 concentrations could induce feedbacks that make the responses different. McCusker et al. (2017) and Oudar et al. (2017) showed the midlatitude response of temperature, sea level pressure, geopotential height, and low-level winds to imposed sea ice loss and global warming due to increased CO_2 were mostly linearly additive in equilibrium,

Denotes content that is immediately available upon publication as open access.

Corresponding author: Tiffany A. Shaw, tas1@uchicago.edu

DOI: 10.1175/JCLI-D-21-0508.1

implying the feedbacks were negligible. However, the importance of feedbacks for the midlatitude storm-track response, including its linearity, have not been quantified. Furthermore, it is unclear if the same mechanism controls the storm-track response to imposed sea ice loss and sea ice loss due to melting.

A useful tool for understanding mechanisms is the climate model hierarchy (Held 2005; Shaw et al. 2016; Polvani et al. 2017; Maher et al. 2019). The midlatitude response to polar amplification has been studied across the model hierarchy. For example, previous studies have focused on the role of dry dynamics (Butler et al. 2010; McGraw and Barnes 2016; Ronalds and Barnes 2019), the stratosphere (Wu and Smith 2016), moisture and the Clausius–Clapeyron relation (Merlis and Henry 2018), insolation conditions (Kim et al. 2018), time scale of adjustment (Hell et al. 2020), and thermal structure (Yuval and Kaspi 2020). While those studies demonstrated an impact of polar amplification on the midlatitudes, they did not connect the midlatitude response to mechanisms that depend on sea ice parameters (sea ice thickness, extent, and surface albedo) because their simulations did not explicitly include sea ice.

Here we use slab-ocean aquaplanet simulations with thermodynamic sea ice from Shaw and Graham (2020) to understand the midlatitude response to sea ice loss. The aquaplanet setup allows for straightforward definitions of imposed sea ice loss (difference without and with sea ice with historical CO_2 concentration) and sea ice loss due to melting (difference of the response to quadrupled CO_2 with and without sea ice). We focus on the midlatitude storm-track intensity response to sea ice loss and use mechanistic frameworks to understand it. We test an energetic mechanism that predicts a weakening of storm-track intensity in response to sea ice loss given the change of surface albedo (a sea ice–dependent parameter) and assuming a passive (slab) ocean. We also quantify the importance of feedbacks for the response to sea ice loss due to melting. Finally, the aquaplanet response to sea ice loss is compared to that from more complex models in the climate model hierarchy.

2. Methods

a. Frameworks

To understand the midlatitude storm-track intensity response to sea ice loss we use two complementary frameworks. The first is the moist static energy (MSE) framework for storm-track intensity (Shaw et al. 2018), which is based on the annual-mean vertically integrated MSE budget of the atmosphere in flux form [global mean removed, see (2) in Kang et al. 2008]:

$$\boldsymbol{\nabla}\cdot F_{\mathrm{TE}} = \underbrace{\boldsymbol{\nabla}\cdot F_{\mathrm{Ra}} + \boldsymbol{\nabla}\cdot F_{\mathrm{TF}}}_{=\boldsymbol{\nabla}\cdot F_{\mathrm{NE}}} - \boldsymbol{\nabla}\cdot F_{\mathrm{SC}}, \tag{1}$$

where all terms have the unit of W m^{-2}, $F_{\mathrm{TE}} = \langle[\overline{v'm'}]\rangle$ and $F_{\mathrm{SC}} = \langle[\overline{v}\,\overline{m}]\rangle$ are the MSE flux by transient eddies and stationary circulation (mean meridional circulation plus stationary eddies), respectively, $\boldsymbol{\nabla}\cdot F_{\mathrm{Ra}} = \mathrm{Ra}$, $\boldsymbol{\nabla}\cdot F_{\mathrm{TF}} = \mathrm{TF}$, and $\boldsymbol{\nabla}\cdot F_{\mathrm{NE}} = \mathrm{NE}$ are in flux form (Ra, TF, and NE have their global mean removed) where Ra is radiative cooling (difference of top of atmosphere and surface radiative fluxes), TF is surface turbulent fluxes (sensible plus latent heat flux), and NE is net energy input to the atmosphere, $\langle\cdots\rangle$ denotes a mass-weighted vertical integration, $[\cdots]$ denotes a zonal average, and $\overline{\cdot}$ denotes a monthly average. The global mean is removed to emphasize meridional gradients (Kang et al. 2008; Donohoe and Battisti 2012; Shaw et al. 2018).

The equation for storm-track intensity [$I(\phi) = 2\pi a\cos\phi F_{\mathrm{TE}}(\phi)$] is obtained by integrating the MSE budget (1) from the pole to latitude ϕ and multiplying by $2\pi a$ (a is the radius of Earth):

$$\begin{aligned} I(\phi) &= 2\pi a\cos\phi\left[F_{\mathrm{Ra}}(\phi) + F_{\mathrm{TF}}(\phi) - F_{\mathrm{SC}}(\phi)\right] \\ &= I_{\mathrm{Ra}}(\phi) + I_{\mathrm{TF}}(\phi) - I_{\mathrm{SC}}(\phi), \end{aligned} \tag{2}$$

where all terms have the unit of PW [see (1)–(4) in Shaw and Graham 2020]. Consequently, a change in storm-track intensity between climates (δI) can be written as

$$\delta I = \delta I_{\mathrm{Ra}} + \delta I_{\mathrm{TF}} - \delta I_{\mathrm{SC}}. \tag{3}$$

According to this framework, the change in storm-track intensity (δI) is connected to the change in radiative cooling (δI_{Ra}) and surface turbulent fluxes (δI_{TF}) and offset by the change in the stationary circulation ($-\delta I_{\mathrm{SC}}$).

The second framework is mean available potential energy (MAPE), which is linearly related to vertically integrated eddy kinetic energy (EKE) across a wide range of climates with a constant rescaling factor c determined via a linear regression (O'Gorman and Schneider 2008; Shaw and Graham 2020). According to this framework, the change in EKE (δEKE) can be connected to the change in MAPE (δMAPE), which can be decomposed into contributions due to baroclinicity (δBARO) and stability (δSTAB):

$$\delta\mathrm{EKE} \approx c\delta\mathrm{MAPE} \approx c\delta\mathrm{BARO} + c\delta\mathrm{STAB}, \tag{4}$$

where $c = 4.0$ and all terms have the units of MJ m^{-2} [see (13)–(15) in Shaw and Graham 2020].

The MSE and MAPE frameworks are complementary and are applied diagnostically to quantify and understand the midlatitude storm-track intensity response to sea ice loss [quantities in (3) and (4) are (area weighted) averaged from 30° to 60°]. In addition to the diagnostic approach, the MSE framework can predict the storm-track response to climate change given the climatology and changes in external parameters. For example, Barpanda and Shaw (2017) and Shaw et al. (2018) used the framework to predict the seasonality of storm-track position and intensity (deviation from the annual mean) given modern seasonal insolation. Barpanda and Shaw (2020) used the framework to connect the hemispheric asymmetry of storm-track seasonality to surface heat capacity (mixed layer depth). Shaw and Graham (2020) used the framework to predict the storm-track intensity response to

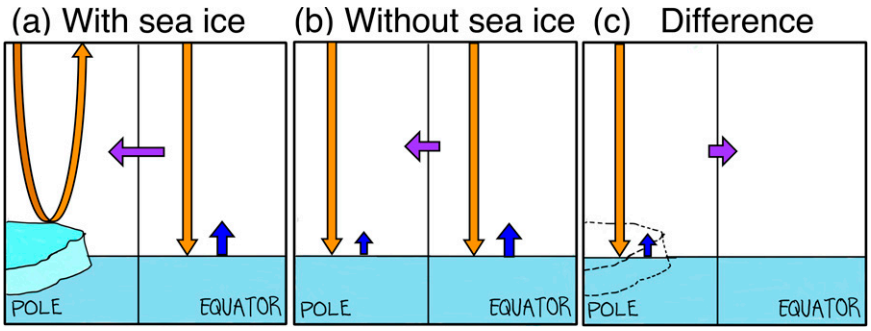

FIG. 1. Energy box model schematic of the climate (a) with sea ice, (b) without sea ice, and (c) the difference, i.e., (b) minus (a). The orange, blue, and purple arrows indicate shortwave radiation, surface turbulent fluxes, and advection (poleward atmospheric energy transport), respectively.

snowball Earth conditions given the modern climate and the Clausius–Clapeyron relation. These predictions give confidence in our understanding of the underlying mechanisms. Note we cannot predict the storm-track response a priori using MAPE because it depends on temperature, which is not an external parameter (it is part of the solution not part of the input).

Here we predict the annual-mean midlatitude storm-track intensity response to sea ice loss given the climatology and the change in surface albedo. The energetic mechanism underlying the prediction is summarized qualitatively using energy box model schematics for hemispheres with and without polar sea ice (Fig. 1). The box model does not account for changes in the global mean climate since the MSE framework (1) only depends on deviations from the global mean (changes in the meridional gradient). The hemispheric box is divided into a poleward side and equatorward side with the midlatitudes in the middle. In the box model the arrows represent different forms of energy transfer (radiation, surface turbulent fluxes, and advection). For simplicity, the box model assumes the following: 1) sea ice is a perfect reflector of shortwave radiation; 2) a passive (slab) ocean boundary condition (no land), including thermodynamic coupling between the atmosphere and ocean but no dynamic coupling; 3) the ocean is a perfect absorber of shortwave radiation; and 4) radiative changes are dominated by shortwave radiation (the change in longwave radiation is assumed to be negligible).

In the climate with sea ice (Fig. 1a), shortwave radiative energy transfer (orange arrow) reflects off of sea ice on the poleward side of the box and is absorbed by the ocean on the equatorward side. Surface turbulent fluxes (blue arrow) are large on the equatorward side and assumed to be negligible on the poleward side of the box because sea ice limits the exchange of energy with the atmosphere. Advection (purple arrow) transfers energy from the equatorward to poleward side of the box consistent with the equator-to-pole imbalance of net energy input to the atmosphere (more energy input on the equatorward side).

In the climate without sea ice (Fig. 1b), shortwave radiation is absorbed by the ocean, which drives increased surface turbulent fluxes (evaporation) into the atmosphere on the poleward side of the box. The shortwave radiation and surface turbulent fluxes are similar to the climate with ice on the equatorward side. Advection transfers energy from the equatorward to poleward side of the box; however, it is weaker than for the climate with sea ice consistent with the weaker equator-to-pole imbalance of net energy input to the atmosphere. Thus, in response to sea ice loss (Fig. 1c) the atmosphere gains energy on the poleward side of the box via the increase of surface turbulent fluxes. Note there is no net effect of the change in shortwave radiation because the change in top of atmosphere fluxes cancel changes at the surface. As a consequence of this increase of net energy input to the atmosphere on the poleward side of the box, the equator-to-pole gradient is weakened relative to the climate with ice and the advection response is equatorward, that is, a weakening of poleward atmospheric energy transport (advection arrow changes direction in Fig. 1c). If we assume the midlatitude storm tracks dominate the advection response, then the box model predicts a weakening of storm-track intensity in response to sea ice loss.

The energetic mechanism can be made quantitative as follows: At the surface, the mechanism assumes the surface turbulent flux response to imposed sea ice loss balances the net surface shortwave radiation response. Thus, the annual-mean surface energy budget response to sea ice loss becomes

$$\delta \mathrm{TF} = \delta \mathrm{SW}_s + \delta \mathrm{LW}_s - \delta \mathrm{NA} \tag{5}$$

$$\approx \delta \mathrm{SW}_s, \tag{6}$$

where all terms have units of W m^{-2}; δTF is the surface turbulent flux response; $\delta \mathrm{SW}_s$ and $\delta \mathrm{LW}_s$ are the net surface shortwave and net surface longwave radiation responses, respectively; and δNA is the nonatmospheric (NA) response. NA processes include ocean and ice energy flux divergence, that is, NA = $O + I$ where O and I are the ocean and ice contributions, respectively (see appendix in Kay et al. 2012). In (6), $\delta \mathrm{LW}_s$ and δNA are assumed to be negligible consistent with the box model.

The net surface shortwave radiation response depends on the surface albedo (α_s) and shortwave optical depth (τ_s), thus

$$\delta \mathrm{TF} \approx \delta \mathrm{SW}_s = \delta\left[(1-\alpha_s)\mathrm{SW}_s^{\downarrow}\right] = \delta\left[(1-\alpha_s)e^{-\tau_s}\mathrm{SW}_t^{\downarrow}\right] \quad (7)$$

$$\approx (1-\alpha_{s,ni})e^{-\tau_{s,ni}}\mathrm{SW}_t^{\downarrow} - (1-\alpha_{s,i})e^{-\tau_{s,i}}\mathrm{SW}_t^{\downarrow}, \quad (8)$$

where the subscripts *ni* and *i* refer to the climate without and with sea ice, respectively; $\mathrm{SW}_s^{\downarrow}$ is the incoming shortwave radiation at the surface; and $\mathrm{SW}_t^{\downarrow}$ is the incoming shortwave radiation at the top of the atmosphere, which is unchanged.

The predicted change in surface turbulent fluxes $\delta\mathrm{TF}_p$ (where the subscript p refers to prediction) given the climatology with sea ice and the change of surface albedo ($\delta\alpha_s = \alpha_{s,ni} - \alpha_{s,i}$) and assuming the change of shortwave optical depth follows the change in surface albedo ($\tau_{s,ni} = \tau_{s,i} - \delta\alpha_s$) is

$$\delta \mathrm{TF}_p \approx \delta \mathrm{SW}_{sp} \approx (1-\alpha_{s,ni})e^{-(\tau_{s,i}-\delta\alpha_s)}\mathrm{SW}_t^{\downarrow} - (1-\alpha_{s,i})e^{-\tau_{s,i}}\mathrm{SW}_t^{\downarrow} \quad (9)$$

$$\approx e^{-\tau_{s,i}}\mathrm{SW}_t^{\downarrow}\left[(1-\alpha_{s,ni})e^{\delta\alpha_s} - (1-\alpha_{s,i})\right], \quad (10)$$

which is an increase of surface turbulent fluxes in the polar region where $\delta\alpha_s < 0$.

Finally, following (3), the predicted change in storm-track intensity is

$$\delta I_p \approx 2\pi a \cos(\phi)\delta F_{\mathrm{TF}_p}(\phi), \quad (11)$$

where $\nabla \cdot \delta F_{\mathrm{TF}_p} = \delta \mathrm{TF}_p$ and $\delta\mathrm{TF}_p$ has its global mean removed, assuming $\delta I_{\mathrm{SC}} \approx 0$ and $\delta I_{\mathrm{Ra}} \approx 0$. Thus, (10)–(11) predict a weakening of the storm track in response to polar sea ice loss because sea ice loss weakens the equator-to-pole gradient of surface turbulent fluxes.

b. Simulations across the climate model hierarchy

As discussed in the Introduction, existing idealized climate models (energy balance models, dry dynamical core models, aquaplanet models without sea ice) do not include the necessary ingredients to test the energetic mechanism (sea ice boundary condition and surface turbulent fluxes, i.e., evaporation). Here we introduce a model that is close to the minimal possible level of complexity to test the energetic mechanism, namely, an aquaplanet with thermodynamic sea ice. We compare the aquaplanet response to more complex climate model simulations.

1) AQUAPLANET

We use the ECHAM6 aquaplanet slab ocean (SO) model developed by the Max Planck Institute for Meteorology (Stevens et al. 2013), herein referred to as SO-AQUA. The climates with and without sea ice, herein referred to as ICE and NOICE, are configured by enabling or disabling thermodynamic sea ice in the slab ocean, that is, setting the namelist parameter *lmlo_ice* to be true or false, respectively (Giorgetta et al. 2013). The simulations are identical to those in Shaw and Graham (2020) and have a seasonal cycle with modern obliquity, modern greenhouse gases, and no ocean heat transport. We decrease the slab-ocean mixed layer depth from 50 to 30 m. Note Shaw and Graham (2020) showed mixed layer depths ≤ 20 m produce a snowball Earth.

The SO-AQUA response to imposed sea ice loss is defined as the difference without and with sea ice (NOICE–ICE) with historical CO_2 concentration (348 ppmv). Across the different mixed layer depths, the response to imposed sea ice loss (NOICE–ICE) involves a loss of ~0.25–4 m of sea ice thickness (Fig. 2a), decreased surface albedo (Fig. 2b), polar amplification of 2 m temperature (Fig. 2c), increased midlatitude precipitation (Fig. 2d), and weakening of storm-track intensity (Figs. 2e,f). Note the definition of imposed sea ice loss used here conserves energy. It also does not require adding heat to the model in order to melt sea ice. We choose the 45 m mixed layer depth as the representative SO-AQUA climate (45 m lines, Fig. 2) and compare it to the response to imposed sea ice loss in more complex climate models.

We also examine the midlatitude response to sea ice loss due to melting in SO-AQUA by quadrupling the CO_2 concentration from 348 to 1392 ppmv. The climates with quadrupled CO_2 with and without sea ice are herein referred to as 4xICE and 4xNOICE. The response to sea ice loss due to melting in SO-AQUA is defined as the difference of the response to quadrupled CO_2 with and without sea ice [(4xICE − ICE) − (4xNOICE − NOICE)]. Note sea ice melts completely in SO-AQUA in response to quadrupled CO_2. In all cases the SO-AQUA simulations are run for 40 years with the results based on the last 20 years.

2) COMPLEX CLIMATE MODEL SIMULATIONS

We compare the ECHAM6 SO-AQUA response to the ECHAM6 SO atmosphere general circulation model response (Stevens et al. 2013), herein referred to as SO-GCM. The SO-GCM ICE configuration includes a full land model, seasonal cycle, modern greenhouse gases, 50 m slab ocean, and imposed ocean heat transport. The ocean heat transport is imposed as a qflux calculated from an ECHAM6 Atmospheric Model Intercomparison Project (AMIP)-type experiment. Following the SO-AQUA setup, the NOICE SO-GCM climate is configured by disabling sea ice in the slab ocean, that is, setting the namelist parameter *lmlo_ice* to false and setting the sea ice fraction in the input file to zero.

The SO-GCM response to imposed sea ice loss is defined as the difference without and with sea ice (NOICE – ICE) with historical CO_2 concentration (348 ppmv). In SO-GCM the response to imposed sea ice loss (NOICE – ICE) involves a loss of ~3 m of sea ice thickness (dashed line, Fig. 2a), decreased surface albedo (dashed line, Fig. 2b), polar amplification of 2 m temperature (dashed line, Fig. 2c), increased midlatitude precipitation (dashed line, Fig. 2d), and weakening of storm-track intensity (dashed lines, Figs. 2e,f). We also examine the midlatitude response to sea ice loss due to melting in SO-GCM by quadrupling the CO_2 concentration from 348 to 1392 ppmv. Consistent with SO-AQUA, the SO-GCM response to sea ice loss due to melting is defined as the difference of the response to quadrupled CO_2 with and without sea ice [(4xICE − ICE) − (4xNOICE − NOICE)]. In all cases

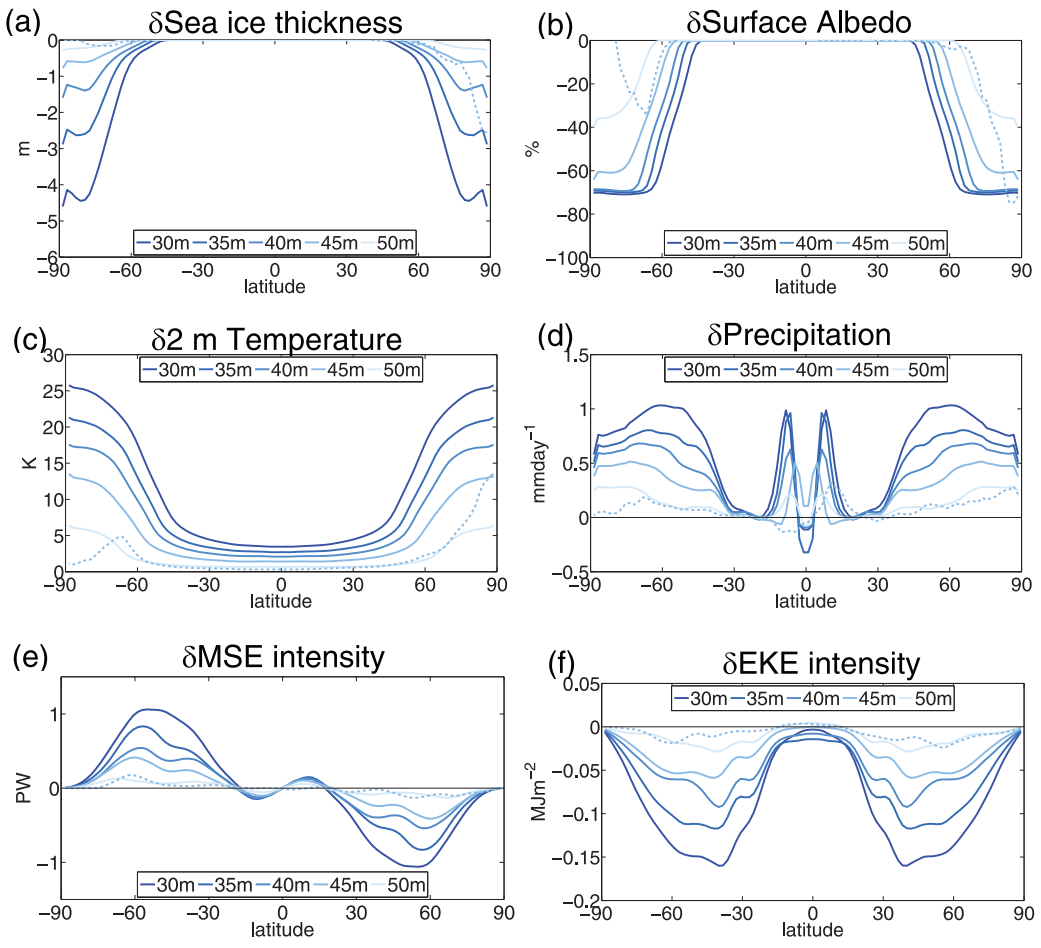

FIG. 2. Annual-mean, zonally averaged (a) sea ice thickness, (b) surface albedo, (c) 2 m temperature, and (d) precipitation, and vertically integrated (e) transient eddy MSE flux and (f) EKE vs latitude in response to imposed sea ice loss (NOICE − ICE) for SO-AQUA (solid) as a function of mixed layer depth (see legend) and SO-GCM (dashed).

the SO-GCM simulations are run for 60 years with the results based on the last 40 years.

Finally, we compare the SO-AQUA and SO-GCM responses, which only include thermodynamic coupling between the atmosphere and ocean, to full ocean (FO) atmosphere general circulation model simulations, which include dynamic coupling between the atmosphere and ocean. We choose two different FO models because they use different methods for imposing sea ice loss. The first FO simulations were performed by England et al. (2020) using the WACCM model, herein referred to as FO-WACCM. The FO-WACCM ICE climate is a 350-yr-long simulation with mid-twentieth-century (1955–69) sea ice conditions. The NOICE climate is a 350-yr-long simulation with future (2085–2099 in the RCP8.5 scenario) sea ice conditions (sea ice loss in both hemispheres). Both the ICE and NOICE simulation have historical forcings (historical CO_2 concentration). Following England et al. (2020) we discard the first 100 years to focus on the equilibrium response. In FO-WACCM sea ice is constrained using the ghost forcing method of Deser et al. (2015). The ghost forcing is imposed as a longwave radiative flux in the sea ice model (it does not directly affect other components) to achieve the desired sea ice concentration and volume in the different time periods (see methods section of England et al. 2020). As discussed in Screen et al. (2018), the ghost forcing method does not conserve energy.

The second FO simulations were performed by Blackport and Kushner (2017) using the CESM model, herein referred to as FO-CESM. The FO-CESM ICE climate is a 725-yr-long simulation with radiative forcing corresponding to year 2000 (historical CO_2 concentration). The FO-CESM NOICE climate is configured by altering sea ice albedo parameters in the sea ice code that allow sea ice to absorb more shortwave radiation and melt in both hemispheres (see section 2 of Blackport and Kushner 2016). As discussed in Screen et al. (2018), the albedo method conserves energy but the imposed albedo may be unphysical. Since only monthly data are available for both FO simulations, we cannot directly quantify the midlatitude storm-track intensity response.

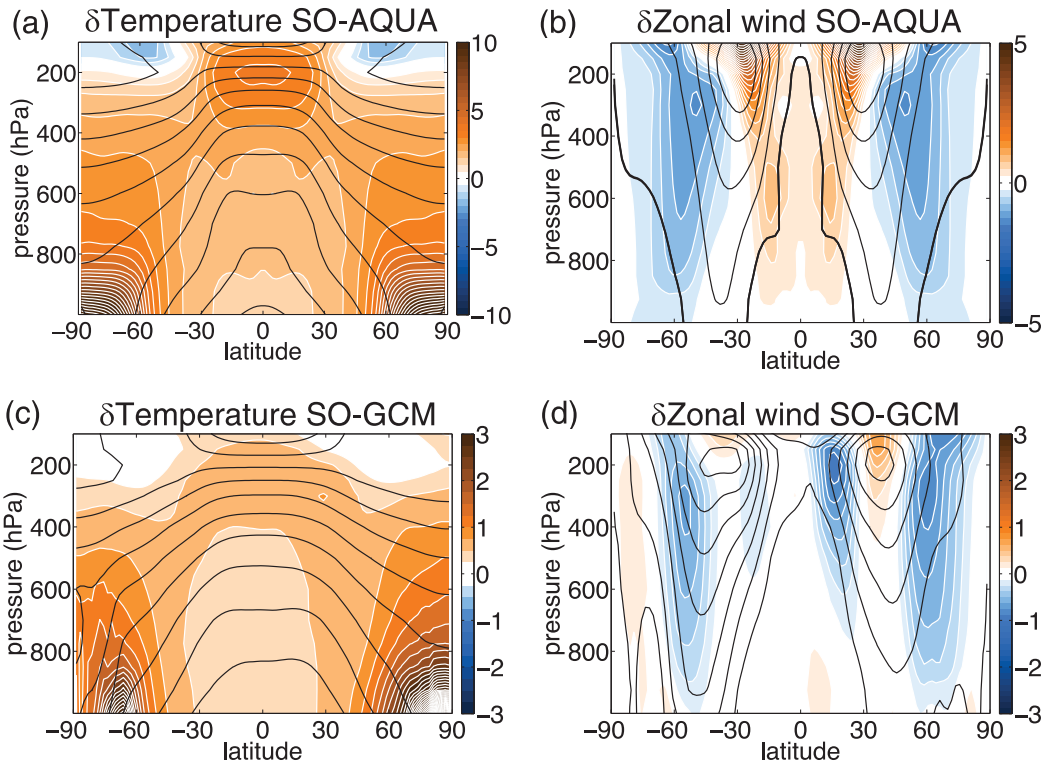

FIG. 3. Annual-mean, zonally averaged (a),(c) temperature (contour interval is 0.5 K for SO-AQUA and 0.25 K for SO-GCM) and (b),(d) zonal wind (contour interval is 0.25 m s^{-1} for SO-AQUA and 0.125 m s^{-1} for SO-GCM) response to imposed sea ice loss (NOICE − ICE) for (a),(b) SO-AQUA and (c),(d) SO-GCM. The black contours indicate the climatology with sea ice.

3. Results

a. Response to imposed sea ice loss

We begin by quantifying the annual-mean, zonal-mean response to imposed sea ice loss (NOICE – ICE) in the representative SO-AQUA simulation (45 m mixed layer depth) and compare it to the SO-GCM, FO-WACCM and FO-CESM responses. The annual-mean response to imposed sea ice loss in the SO-AQUA simulation includes

- global-mean warming (3.0 K),
- amplified tropical warming aloft and polar amplified warming at the surface (Fig. 3a),
- weakening of the near-surface zonal wind in high latitudes (Fig. 3b),
- increased extratropical precipitation that is polar amplified (45 m line, Fig. 2d), and
- weakening of storm-track intensity as measured by vertically integrated transient eddy MSE flux (45 m line, Fig. 2e) or EKE (45 m line, Fig. 2f).

All of these responses are in qualitative agreement with the SO-GCM response to imposed sea ice loss. For example, in response to imposed sea ice loss in SO-GCM there is global-mean warming of 1.1 K and the temperature, zonal wind and storm-track intensity responses are comparable (cf. 45 m to dashed line in Figs. 2 and 3a–d). In addition, the SO-AQUA and SO-GCM temperature and zonal wind responses qualitatively agree with the FO-WACCM response as shown in Figs. 3 and 4 of England et al. (2018) and Fig. 1 of England et al. (2020) and the FO-CESM response as shown in Fig. 4 of Blackport and Kushner (2017).

STORM-TRACK INTENSITY RESPONSE TO IMPOSED SEA ICE LOSS

The midlatitude storm-track intensity (vertically integrated transient eddy MSE flux or EKE) weakens in response to imposed sea ice loss in SO-AQUA across the different mixed layer depths (black bars, Figs. 4a,b). When the weakening of the midlatitude storm-track intensity is decomposed into different contributions following the MSE framework (3), the surface turbulent flux contribution dominates (blue bars, Fig. 4a). The contributions from radiative cooling (orange bars, Fig. 4a) and the stationary circulation (red bars, Fig. 4a) are small.

The predicted weakening of the midlatitude storm-track intensity following the energetic mechanism, that is, (5)–(11), is reasonably accurate (cf. dark and light blue bars, Fig. 4a). This is consistent with the significant correlation between the weakening of storm-track intensity and the sea ice edge in

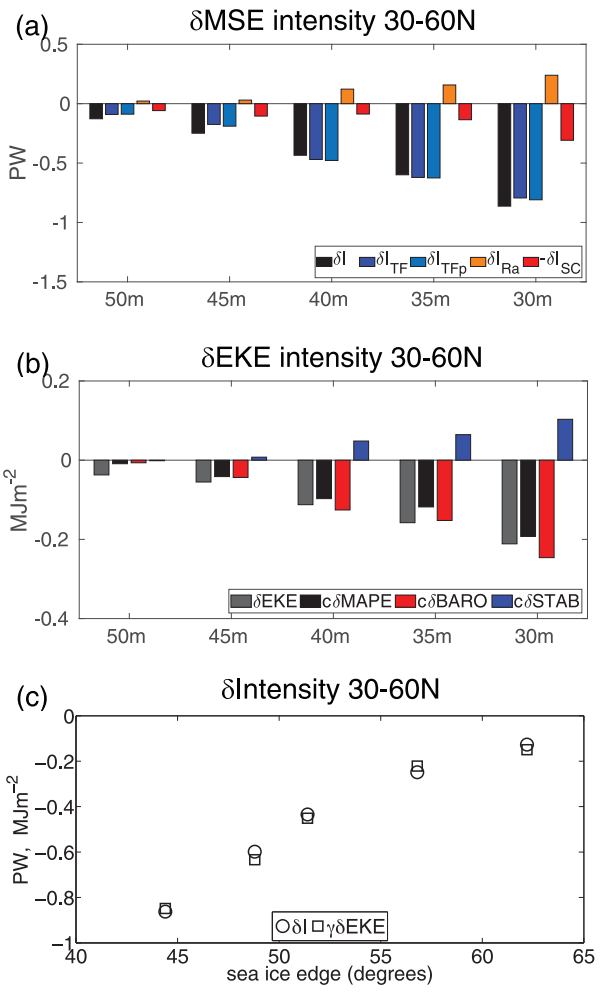

FIG. 4. Annual-mean midlatitude (30°–60°) storm-track (a) MSE (δI) and (b) EKE (δEKE) intensity response to imposed sea ice loss for different mixed layer depths (x axis) in SO-AQUA. In (a) δI (y axis) is decomposed into contributions from surface turbulent fluxes (δI_{TF}), including its prediction (δI_{TF_p}), radiative cooling (δI_{Ra}) and stationary circulation ($-\delta I_{\mathrm{SC}}$) (see legend). In (b), δEKE response and MAPE response ($c\delta$MAPE) where $c = 4$ decomposed into contributions from baroclinicity ($c\delta$BARO) and stability ($c\delta$STAB) (see legend). (c) Storm-track intensity response in (a) and (b) to imposed sea ice loss vs sea ice edge (latitude where the surface albedo change is less than zero). EKE intensity is rescaled $\gamma = 4$.

response to sea ice loss across the different mixed layer depths (open circles, Fig. 4c). Overall, the results demonstrate a quantitative connection between the weakening of storm-track intensity in response to imposed sea ice loss and surface albedo (a sea ice–dependent parameter).

The weakening of EKE in response to imposed sea ice loss is significantly correlated with the weakening of MAPE rescaled by a factor of $c = 4.0$ ($R = 0.99$). The weakening of MAPE (black bars, Fig. 4b) follows the change in baroclinicity (red bars, Fig. 4b) rather than stability (blue bars, Fig. 4b). The weakening of EKE is significantly correlated with the sea ice edge (open squares, Fig. 4c). This reflects the significant correlation between storm-track intensity defined using EKE and the transient eddy MSE flux ($R = 0.99$).

The results suggest the weakening of the midlatitude storm-track intensity in response to imposed sea ice loss in SO-AQUA is diagnostically related to the increase of surface turbulent fluxes in the polar region and to the decrease of baroclinicity (polar amplification). Next, we further examine the assumptions underlying the energetic mechanism (Fig. 1) and test its quantitative prediction, that is, (5)–(11), across the climate model hierarchy. Recall the energetic mechanism underlying the prediction assumes the surface turbulent flux response to imposed sea ice loss balances the net surface shortwave radiation response in the polar region because the surface longwave radiation and nonatmospheric responses are negligible. This weakens the equator-to-pole gradient of net energy input to the atmosphere and thereby weakens the poleward atmospheric energy transport and the storm-track intensity.

The surface energy budget response to imposed sea ice loss in SO-AQUA confirms the net surface shortwave radiation response largely balances the surface turbulent flux response in the polar region (cf. orange and solid blue lines poleward of 60°, Fig. 5a). The net surface longwave radiation and nonatmospheric responses are negligible in the polar region (green and light blue lines, Fig. 5a). The predicted surface turbulent flux response, that is, (10), captures the increase in the polar region but underestimates its amplitude (cf. solid and dashed blue lines, Fig. 5a). The underestimation occurs because the predicted shortwave optical depth response is an overestimate ($|\delta\tau_s| < |\delta\alpha_s|$, not shown).

The surface energy budget response to imposed sea ice loss in SO-GCM agrees qualitatively with SO-AQUA. More specifically, the net surface shortwave radiation response largely balances the surface turbulent flux response in the polar region (cf. orange and solid blue lines, Fig. 5b) and the nonatmospheric response is small (light blue line, Fig. 5b). However, the net surface longwave radiation response in SO-GCM is larger than in SO-AQUA (cf. green lines, Figs. 5a,b). The difference may be related to the vertical structure of the temperature response because the downward surface longwave radiation response is smaller than the upward surface longwave radiation response in SO-GCM (they have a similar magnitude in SO-AQUA). In particular, polar amplification in response to imposed sea ice loss in SO-AQUA is trapped near the surface, whereas it extends into the free troposphere in SO-GCM (cf. Figs. 3a,c). The predicted response of surface turbulent fluxes, that is, (10), in SO-GCM captures the increase in the polar region (cf. solid and dashed blue lines, Fig. 5b).

The surface energy budget response in the FO simulations depends on the method used to impose sea ice loss. In particular, in FO-WACCM, where sea ice loss is imposed using the ghost forcing method, the net surface shortwave radiation response partly balances the surface turbulent flux response in the polar region (cf. orange and solid blue lines, Fig. 5c). However, the nonatmospheric response is also important and partly balances the surface turbulent flux response (light blue line,

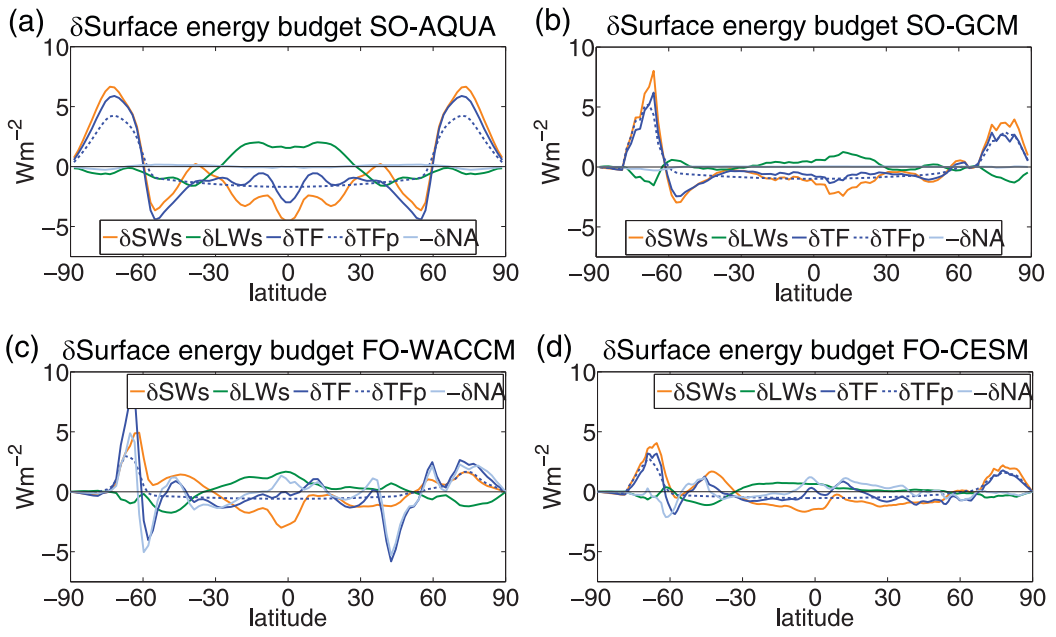

FIG. 5. Annual-mean, zonally averaged cosine-weighted flux form (each term has global mean removed) surface energy budget response to imposed sea ice loss decomposed into net shortwave radiation (δSW_s), net longwave radiation (δLW_s), surface turbulent flux (δTF) and nonatmospheric ($-\delta NA$) contributions for (a) SO-AQUA, (b) SO-GCM, (c) FO-WACCM, and (d) FO-CESM. The blue dashed lines indicate the predicted surface turbulent flux response (δTF_p) [see (10)].

Fig. 5c) but is opposed by the net surface longwave radiation response (green line, Fig. 5c). In FO-WACCM the predicted response of surface turbulent fluxes, that is, (10), captures the increase in the polar region but underestimates its amplitude because it neglects the nonatmospheric response (cf. solid and dashed blue lines, Fig. 5c).

In FO-CESM, where sea ice loss is imposed using the albedo method, the net surface shortwave radiation response largely balances the surface turbulent flux response in the polar region (cf. orange and solid blue lines, Fig. 5d). The net surface longwave radiation and nonatmospheric responses in the polar region are mostly negligible, especially in the Northern Hemisphere (green and light blue lines, Fig. 5d). The predicted response of surface turbulent fluxes, that is, (10), in FO-CESM captures the increase in the polar region (cf. solid and dashed blue lines, Fig. 5d).

The FO simulations show that the method used to impose sea ice loss in coupled models significantly impacts the surface energy budget response, in particular the nonatmospheric response in the polar region. In FO-CESM, the nonatmospheric response is mostly small in the polar region, particularly in the Arctic (light blue line, Fig. 5d). In contrast, the nonatmospheric response in FO-WACCM is large in the polar region and mostly dominated by the ice contribution (maroon line, Fig. 6). The ocean contribution is large around the sea ice edge and is the opposite sign (purple line, Fig. 6). The ice response reflects the ghost forcing in the sea ice model (see section 2a; M. E. England 2021, personal communication). (Note the ice response in Fig. 6 is nonzero outside regions of sea ice because the global-mean was removed.)

The final assumption of the energetic mechanism is that the increase of surface turbulent fluxes in the polar region weakens the equator-to-pole gradient of net energy input to the atmosphere and thereby weakens the poleward atmospheric energy transport. Consequently, the storm-track intensity weakens assuming radiative cooling and stationary circulation changes are small. In SO-AQUA the surface turbulent flux contribution dominates the weakening of storm-track intensity (blue line, Fig. 7a). The radiative cooling and stationary circulation contributions are negligible (orange and red lines, Fig. 7a). The predicted weakening of storm-track intensity,

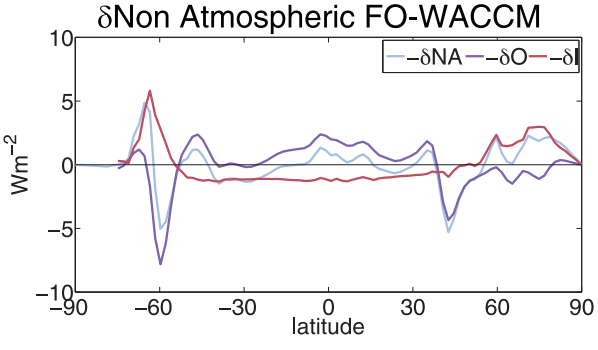

FIG. 6. Annual-mean, zonally averaged nonatmospheric ($-\delta NA$) contribution to the cosine-weighted flux form (each term has the global mean removed) surface energy budget response to imposed sea ice loss decomposed into ocean ($-\delta O$) and ice ($-\delta I$) contributions for FO-WACCM.

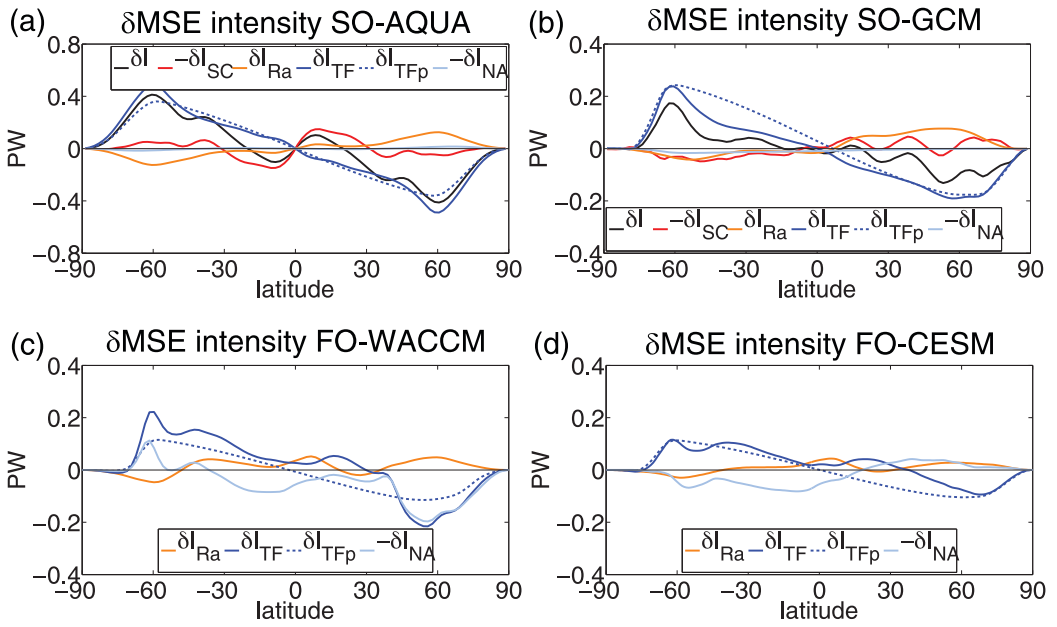

FIG. 7. Annual-mean, zonally averaged MSE intensity response to imposed sea ice loss (δI) decomposed into contributions from the stationary circulation ($-\delta I_{\mathrm{SC}}$), radiative cooling (δI_{Ra}), and surface turbulent fluxes (δI_{TF}) for (a) SO-AQUA, (b) SO-GCM, (c) FO-WACCM, and (d) FO-CESM. The dark blue dashed lines indicate the predicted surface turbulent flux contribution (δI_{TF_p}) in response to imposed sea ice loss given the climatology and change in surface albedo [see (11)]. The light blue lines indicate the nonatmospheric contribution ($-\delta I_{\mathrm{NA}}$) to the surface turbulent flux contribution in response to imposed sea ice loss [see (5)]. FO-WACCM and FO-CESM data were not available to calculate all terms.

that is, (11), underestimates the actual weakening around 60° (blue dashed line, Fig. 7a) consistent with the underestimate of surface turbulent fluxes in the polar region (blue dashed line, Fig. 5a). The predicted weakening is more accurate when (area weighted) averaged over midlatitudes (Fig. 4a) because the polar regions have small area.

The surface turbulent flux contribution dominates the weakening of storm-track intensity in SO-GCM (blue line, Fig. 7b) and the prediction is fairly accurate especially in the Northern Hemisphere (blue dashed line, Fig. 7b). In FO-WACCM and FO-CESM the surface turbulent flux contribution also dominates the weakening of poleward atmospheric energy transport (blue line, Figs. 7c,d). However, the accuracy of the predicted weakening depends on the method used to impose sea ice loss. In particular, it is more accurate in FO-CESM (dashed blue line, Fig. 7d), which uses the albedo method, than in FO-WACCM (dashed blue line, Fig. 7c), which uses the ghost forcing method. The accuracy of the predicted poleward atmospheric energy transport response is tied to the nonatmospheric response. The nonatmospheric response is large and represents a weakening of poleward energy transport for the ghost forcing method (light blue line, Fig. 7c), whereas it is small and represents a strengthening of poleward energy transport for the albedo method (light blue line, Fig. 7d).

The annual-mean response to imposed sea ice loss discussed above reflects distinct seasonal changes. More specifically, the seasonal response of the surface energy budget in SO-AQUA and SO-GCM to imposed sea ice loss shows the net surface shortwave radiation response occurs from spring to summer in the polar region (orange lines, Fig. 8). In contrast, the surface turbulent flux response occurs from fall to winter in the polar region (blue lines, Fig. 8). Ultimately, the seasonal net surface shortwave radiation and surface turbulent flux responses are coupled via ocean (surface) energy storage ($\mathrm{Co}\partial T_s/\partial t$, where Co is the ocean mixed layer heat capacity and T_s is surface temperature; black lines in Fig. 8). In particular, the shortwave radiation energy is absorbed and stored in the surface from spring to summer and is released back to the atmosphere via surface turbulent fluxes from fall to winter. The seasonal response to imposed sea ice loss in the polar region in SO-AQUA and SO-GCM is consistent with previous coupled model results, for example, see Fig. 2 in Deser et al. (2015), Fig. A2 in Blackport and Kushner (2017), and Fig. 2 in Sun et al. (2018).

Seasonally, the weakening of storm-track intensity as measured by vertically integrated transient eddy MSE flux (colored contours, Figs. 9a,b) or EKE (black contours, Figs. 9a,b) in response to imposed sea ice loss is largest from fall to winter in SO-AQUA and SO-GCM. The MSE intensity response clearly follows the seasonal changes of the surface turbulent flux contribution (Figs. 9c,d) consistent with the annual-mean energetic mechanism.

b. Response to sea ice loss due to melting

The response to imposed sea ice loss discussed in the previous subsection was quantified as the difference without and

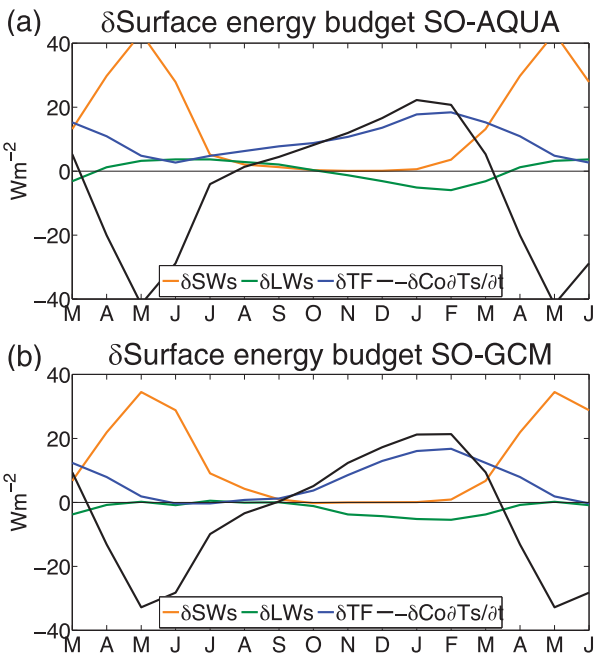

FIG. 8. Seasonal response of the zonally averaged surface energy budget in the polar region to imposed sea ice loss decomposed into net shortwave radiation (δSW_s), net longwave radiation (δLW_s), surface turbulent flux (δTF), nonatmospheric ($-\delta NA$), and ocean (surface) energy storage ($-\delta Co\partial T_s/\partial t$) contributions for (a) SO-AQUA and (b) SO-GCM.

with sea ice with historical CO_2 concentration (NOICE–ICE). In reality, sea ice loss is driven by a forcing, for example, melting due to increased CO_2. As discussed in the introduction, the response to imposed sea ice loss and sea ice loss due to melting could differ because they occur at different CO_2 concentrations. In particular, the higher CO_2 concentration could induce feedbacks, for example, water vapor or cloud feedbacks, that affect the mechanism underlying the response.

Here we quantify the response to sea ice loss due to melting defined as the difference of the response to quadrupled CO_2 with and without sea ice [(4xICE − ICE) − (4xNOICE − NOICE)] and compare it to the response to imposed sea ice loss. If the response to imposed sea ice loss and sea ice loss due to melting are quantitatively similar then it implies feedbacks are small, that is, if (NOICE − ICE) ≈ (4xICE − ICE) − (4xNOICE − NOICE) then 4xICE ≈ 4xNOICE, and the underlying mechanisms are similar. Furthermore, it would imply that the response to quadrupled CO_2 can be decomposed approximately linearly into two parts: 1) the response to quadrupled CO_2 without climatological sea ice (4xNOICE − NOICE), herein referred to as global warming without ice; and 2) the response to sea ice loss due to melting. In what follows, we quantify both parts of the response and the linearity following McCusker et al. (2017).

The annual-mean response to global warming without ice in the SO-AQUA simulation includes

- global-mean warming (4.0 K, solid red line, Fig. 10a),
- amplified tropical warming aloft (Fig. 11a) and no polar amplified warming at the surface (solid red line, Fig. 10a), and
- strengthening of storm-track intensity as measured by vertically integrated transient eddy MSE flux (solid red line, Fig. 10b) or EKE (solid red line, Fig. 10c).

The SO-AQUA storm-track intensity response is in qualitative agreement with the SO-GCM response to global warming without ice (cf. red lines, Figs. 10b,c). The temperature responses differ due to significant warming over land in SO-GCM (cf. red lines, Figs. 10a and 11a,b).

The annual-mean response to sea ice loss due to melting in the representative SO-AQUA simulation includes

- global-mean warming (3.0 K, solid blue line, Fig. 10a),
- amplified tropical warming aloft (Fig. 11c) and polar amplified warming at the surface (solid blue line, Fig. 10a), and
- weakening of storm-track intensity as measured by vertically integrated transient eddy MSE flux (solid blue line, Fig. 10b) or EKE (solid blue line, Fig. 10c).

All of these responses are in qualitative agreement with the SO-GCM response to sea ice loss due to melting (dashed blue lines, Figs. 10 and 11d).

In SO-AQUA the 2 m temperature (solid black line, Fig. 10a), storm-track intensity (solid black lines, Figs. 10b,c), and atmospheric temperature (Fig. 11e) responses are very linear. Thus, the higher CO_2 concentration during sea ice melting does not induce significant feedbacks in SO-AQUA. In SO-GCM the responses of 2 m temperature (dashed black line, Fig. 10a), storm-track intensity (dashed black lines, Figs. 10b,c), and atmospheric temperature (Fig. 11f) are not as linear.

1) STORM-TRACK INTENSITY RESPONSE TO SEA ICE LOSS DUE TO MELTING

We begin by quantifying the annual-mean surface energy budget response to sea ice loss due to melting in order to test the energetic mechanism in the presence of a higher CO_2 concentration. We subsequently quantify the storm-track intensity response. The surface energy budget response to sea ice loss due to melting in SO-AQUA and SO-GCM confirms the net surface shortwave radiation response largely balances the surface turbulent flux response in the polar region (cf. orange and blue lines, Fig. 12). Overall, the response to sea ice loss due to melting (Figs. 12a,b) is very similar to the response to imposed sea ice loss (Figs. 5a,b), hence feedbacks in response to the higher CO_2 concentration are small.

The midlatitude storm-track intensity (as measured by vertically integrated transient eddy MSE flux) weakens in response to sea ice loss due to melting in SO-AQUA and SO-GCM (black lines, Fig. 13), which opposes the strengthening in response to global warming without ice (red lines, Figs. 10b,c). Interestingly, the weakening in response to sea ice loss due to melting is dominated by dry static energy transport in midlatitudes (there is little change in latent energy transport, not shown). In contrast the strengthening in response to sea ice loss due to melting is dominated by latent

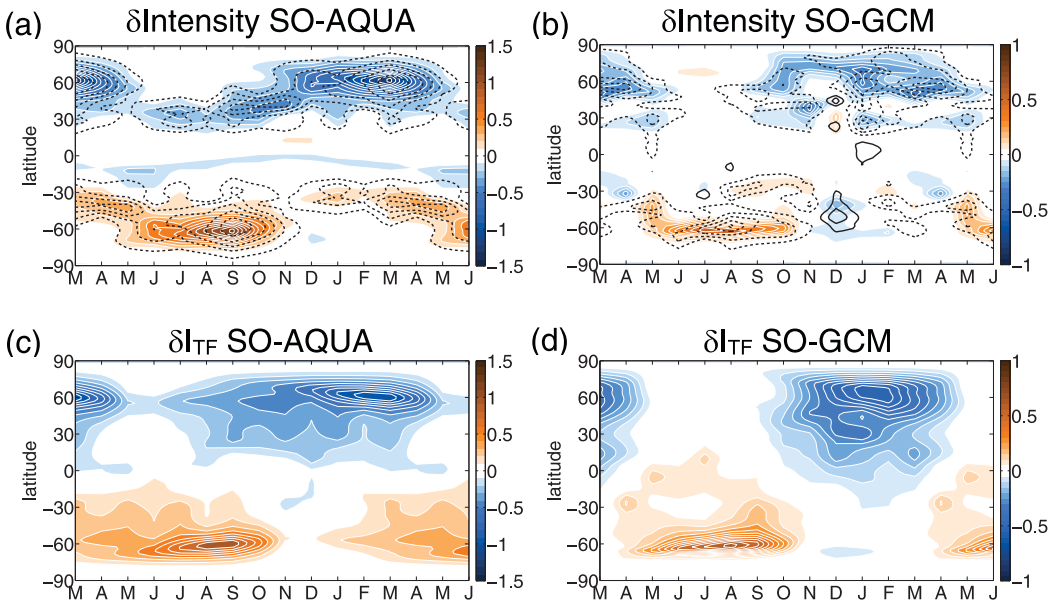

FIG. 9. Seasonal response of zonally averaged (a),(b) vertically integrated transient eddy MSE flux (colored contours, interval: 0.1 PW) and EKE (black contours, interval: 0.025 MJ m^{-2}) storm-track intensity and (c),(d) surface turbulent flux contribution to MSE intensity (colored contours, interval: 0.1 PW) to imposed sea ice loss for SO-AQUA (left) and SO-GCM (right).

energy transport in midlatitudes (the change in dry static energy transport is opposite, not shown).

When the weakening in response to sea ice loss due to melting is decomposed into different contributions following the MSE framework (3), the change in surface turbulent fluxes dominates (blue lines, Fig. 13). The contributions from radiative cooling (orange lines, Fig. 13) and the stationary circulation (red lines, Fig. 13) are small in midlatitudes. This suggests that the equilibrium energetic mechanism explaining the midlatitude response to imposed sea ice loss (Fig. 1) also explains the equilibrium response to sea ice loss due to melting.

2) TRANSIENT RESPONSE TO SEA ICE LOSS DUE TO MELTING

The previous subsection established the equilibrium response to sea ice loss due to melting is quantitatively similar to the equilibrium response to imposed sea ice loss. As discussed by Shaw (2019), quantifying the transient response to forcing is another important tool for testing mechanisms. Here we test whether the energetic mechanism operates transiently in response to sea ice loss due to melting.

The transient response to sea ice loss due to melting in SO-AQUA involves a rapid increase of net surface shortwave radiation and surface turbulent fluxes in the polar region and a negligible change in net surface longwave radiation (Fig. 14a). The time scale of the response in the polar region is consistent with the melting of sea ice, which takes approximately 6 years. The transient response in SO-GCM also involves a rapid increase of net surface shortwave radiation and surface turbulent fluxes; however, the net surface longwave radiation response is larger (Fig. 14b). The time scale of the response in SO-GCM is slightly longer than SO-AQUA, consistent with a longer time scale for the melting of sea ice, which takes approximately 10 years in SO-GCM. Overall the transient surface response to sea ice loss due to melting is consistent with the equilibrium surface response to sea ice loss (see Figs. 5 and 12).

The storm-track intensity weakens transiently in response to sea ice loss due to melting in SO-AQUA (black lines, Fig. 14c). The transient weakening follows the surface turbulent flux contribution in the MSE framework (blue line, Fig. 14c). The radiative cooling (orange lines, Fig. 14c) and stationary circulation (red lines, Fig. 14c) contributions are small. A similar transient response to sea ice loss due to melting is seen in SO-GCM (Fig. 14d). Overall the results suggest the energetic mechanism operates transiently in response to sea ice loss due to melting.

4. Conclusions and discussion

a. *Conclusions*

Slab-ocean aquaplanet simulations with thermodynamic sea ice are used to study the zonally symmetric mechanisms whereby polar sea ice loss impacts the midlatitude atmosphere. Our conclusions are as follows:

- The response to imposed sea ice loss (difference without and with sea ice with historical CO_2 concentration) includes global warming, polar amplified warming, weakening of poleward atmospheric energy transport, and the midlatitude storm-track intensity.

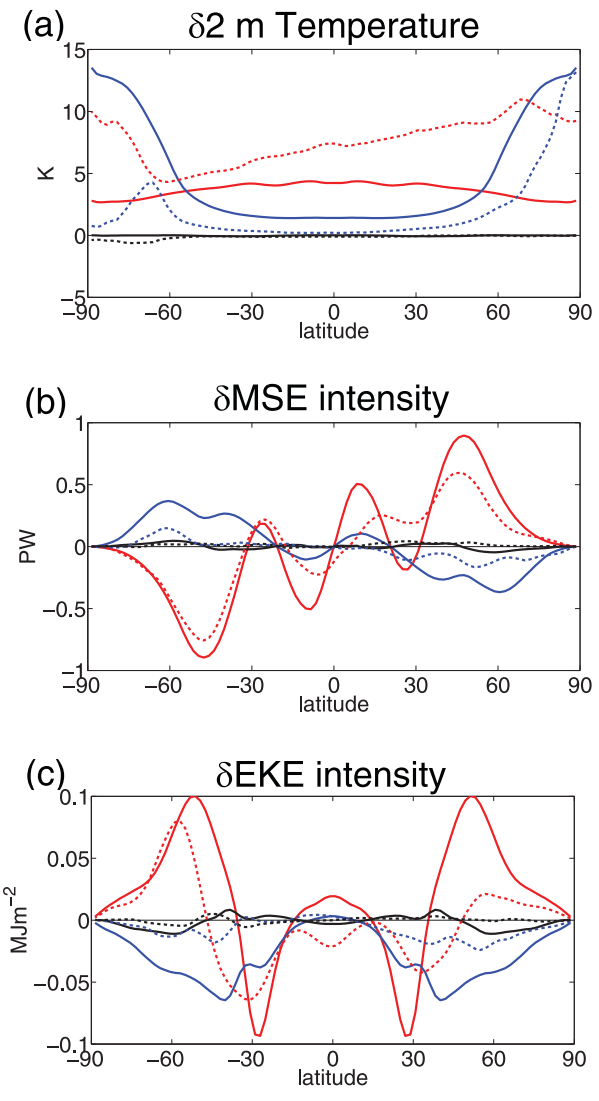

FIG. 10. Annual-mean, zonally averaged (a) 2 m temperature and vertically integrated (b) transient eddy MSE flux and (c) EKE response to global warming without ice (4xNOICE − NOICE, red), sea ice loss due to melting [(4xICE − ICE) − (4xNOICE − NOICE), blue] and the nonlinearity (4xICE − 4xNOICE, black) for SO-AQUA (solid) and SO-GCM (dashed).

- The weakening of the midlatitude storm-track intensity in response to imposed sea ice loss is consistent with increased surface turbulent fluxes in the polar region (decreased equator-to-pole gradient of net energy input to the atmosphere) and decreased MAPE (decreased baroclinicity due to polar amplified warming). The changes in radiative cooling, stationary circulation, and stability do not contribute significantly to the weakening.
- The simulations confirm the following energetic mechanism that predicts a weakening of storm-track intensity in response to imposed sea ice loss assuming a passive (slab) ocean. Sea ice loss decreases the surface albedo in the polar region thereby increasing the absorption of shortwave radiation at the surface, which drives an increase in surface turbulent fluxes into the atmosphere. Consequently, energy input to the atmosphere in the polar region increases, thereby weakening poleward atmospheric energy transport and the storm-track intensity. The quantitative prediction underlying the mechanism, which assumes the change of shortwave optical depth follows the change in surface albedo, captures the weakening but underestimates its amplitude.
- Consistent with the energetic mechanism, the weakening of storm-track intensity in response to imposed sea ice loss scales with the sea ice edge (latitude where the change of surface albedo is less than zero), which is controlled by the slab-ocean depth.
- The equilibrium response to sea ice loss due to melting (difference of the response to quadrupled CO_2 with and without sea ice) is very similar to the response to imposed sea ice loss. This suggests that feedbacks in response to the higher CO_2 concentration do not significantly affect the midlatitude storm-track intensity response. The weakening of storm-track intensity in response to sea ice loss due to melting opposes the strengthening in response to global warming without sea ice.
- The energetic mechanism explains the equilibrium and transient response to sea ice loss due to melting.

The aquaplanet results above were shown to be qualitatively consistent with the response in more complex climate models. In particular, the energetic mechanism operates qualitatively across the model hierarchy (even in the presence of dynamic coupling between the atmosphere and ocean). More specifically, in the polar region the surface turbulent flux response to imposed sea ice loss is mostly balanced by the net surface shortwave radiation response, and the change in surface turbulent flux dominates the weakening of storm-track intensity across the model hierarchy. However, in coupled climate models the method used to impose sea ice loss impacts the surface energy budget response and the accuracy of the quantitative prediction underlying the energetic mechanism. In particular, the prediction is more accurate when the albedo method is used to impose sea ice loss because it involves a small nonatmospheric response to sea ice loss in the polar region. The prediction is less accurate when the ghost forcing method is used because it involves a large nonatmospheric response to sea ice loss in the polar region. Overall, the results show aquaplanet simulations with thermodynamic sea ice are a useful tool for understanding the mechanisms underlying the response to sea ice loss in more complex climate models. They fill an important gap in the climate model hierarchy for understanding the interaction between polar climate and the midlatitude atmosphere.

b. *Discussion*

Slab-ocean aquaplanet simulations with thermodynamic sea ice qualitatively capture many of the responses to imposed sea ice loss in more complex climate models, that is, global warming, polar amplified warming, weakening of poleward atmospheric energy transport, weakening and equatorward shift of the eddy driven jet, and equatorward shift of the

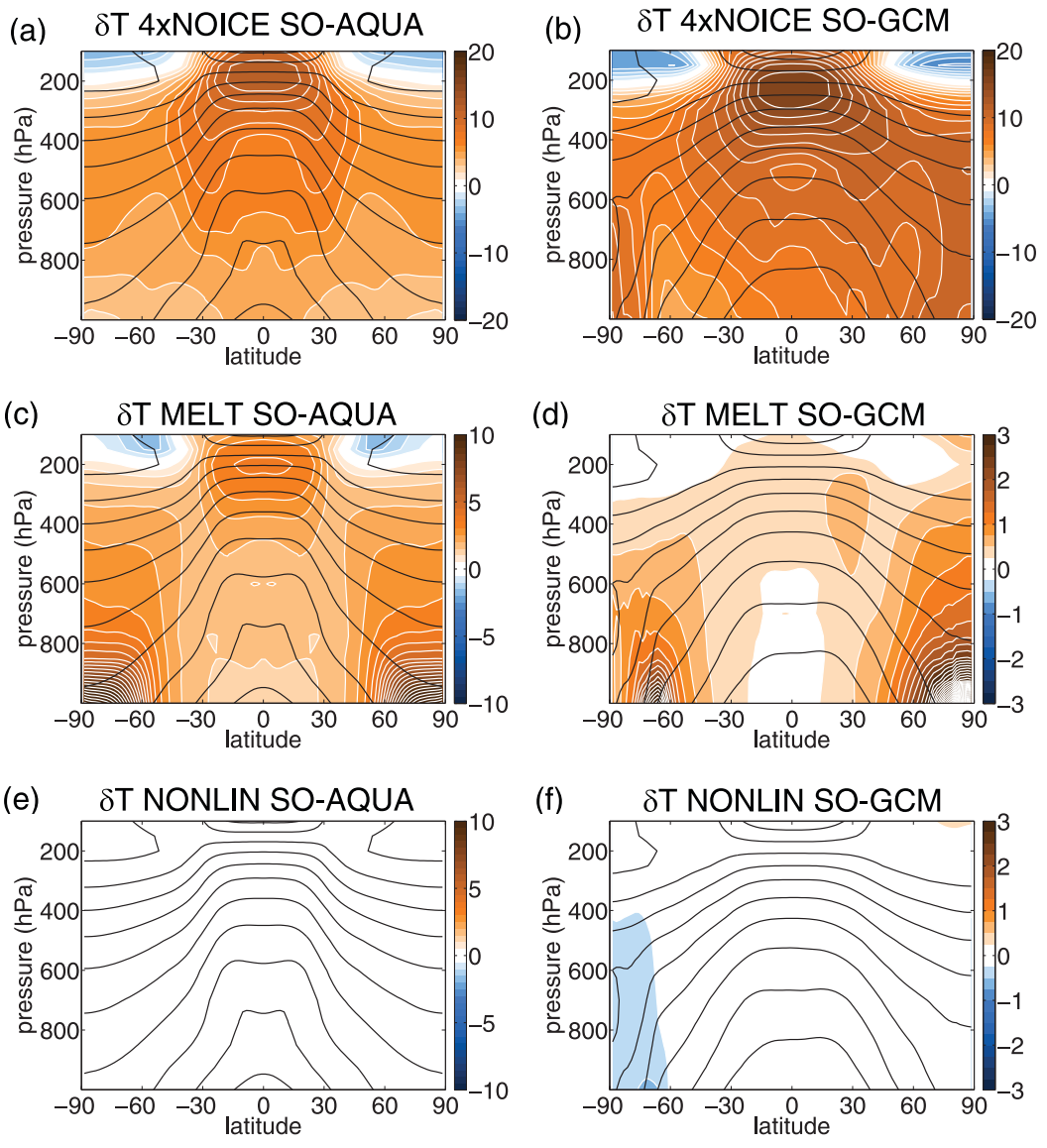

FIG. 11. Annual-mean, zonally averaged temperature response to (a),(b) global warming without ice (4xNOICE − NOICE, contour interval: 1 K), (c),(d) sea ice loss due to melting [(4xICE − ICE) − (4xNOICE − NOICE), contour interval is 0.5 K in SO-AQUA and 0.25 K in SO-GCM] and (e),(f) the nonlinearity [4xICE − 4xNOICE, contour interval as in (c) and (d)] for SO-AQUA (left) and SO-GCM (right). The black contours indicate the climatology with sea ice.

ITCZ (e.g., Deser et al. 2015; Blackport and Kushner 2017; McCusker et al. 2017; England et al. 2018; Screen et al. 2018; England et al. 2020). In addition, the aquaplanet simulations capture the tug-of-war on storm-track intensity between sea ice loss and global warming (dominated by water vapor feedback) seen in complex climate models (Harvey et al. 2014; Barnes and Screen 2015; Harvey et al. 2015; Shaw et al. 2016; Audette et al. 2021). The tug-of-war also occurs for poleward atmospheric energy transport consistent with coupled climate models (Hwang and Frierson 2010).

The linearity of the zonally symmetric midlatitude storm-track intensity response to imposed sea ice loss and sea ice loss due to melting is consistent with the linearity reported in coupled climate models (Oudar et al. 2017; McCusker et al. 2017). Since the zonally symmetric aquaplanet configuration has helped to uncover the zonally symmetric mechanisms whereby sea ice loss impacts the midlatitudes, future work could focus on using the aquaplanet to simulate and understand the zonally asymmetric response to sea ice loss, for example, the warm Arctic–cold Eurasia pattern (Screen et al. 2018; Labe et al. 2020).

The slab-ocean aquaplanet allows for thermodynamic coupling between the atmosphere and ocean but neglects dynamic coupling. Consistent with previous work, thermodynamic coupling is

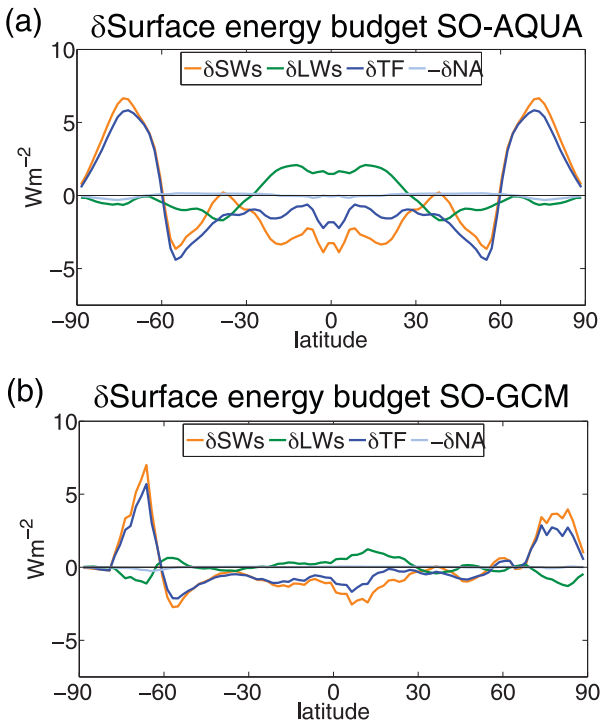

FIG. 12. Annual-mean, zonally averaged cosine-weighted flux form (each term has the global mean removed) surface energy budget response to sea ice loss due to melting decomposed into net shortwave radiation (δSW_s), net longwave radiation (δLW_s), surface turbulent flux (δTF), and nonatmospheric ($-\delta NA$) contributions for (a) SO-AQUA and (b) SO-GCM.

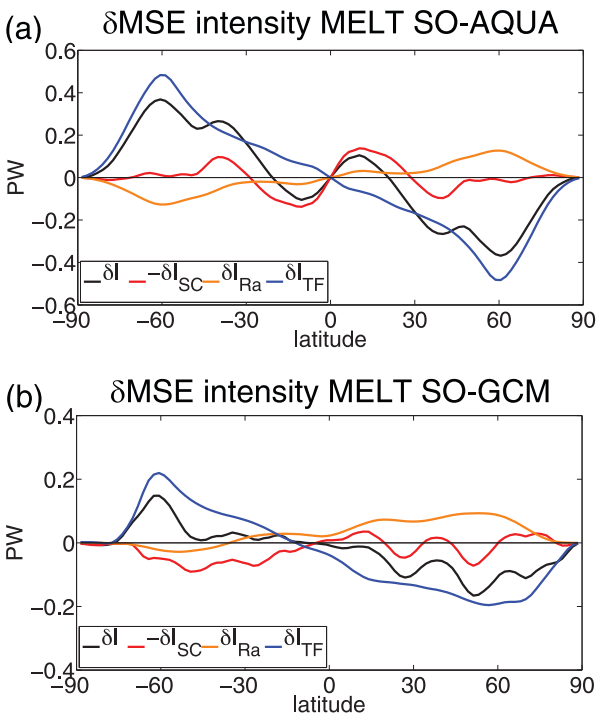

FIG. 13. Annual-mean, zonally averaged MSE intensity response (δI) to sea ice loss due to melting [(4xICE − ICE) − (4xNOICE − NOICE)] decomposed into contributions from stationary circulation ($-\delta I_{SC}$), radiative cooling (δI_{Ra}) and surface turbulent flux (δI_{TF}) for (a) SO-AQUA and (b) SO-GCM.

sufficient to qualitatively capture many of the responses to sea ice loss (Deser et al. 2015, 2016; Tomas et al. 2016; Wang et al. 2018). In the presence of dynamic coupling between the atmosphere and ocean, the results show the energetic mechanism still operates, however, the accuracy of the prediction underlying the mechanism depends on the method used to impose sea ice loss in coupled models. The prediction is more accurate when using the albedo method and is less accurate when using the ghost forcing method. More work is needed to understand whether this is related to the fact that the albedo method conserves energy whereas the ghost forcing method does not (Screen et al. 2018). Sun et al. (2020) showed one can simulate similar atmospheric responses (temperature, surface pressure, precipitation) using the different methods; however, they did not compare the surface shortwave radiation, nonatmospheric, and storm-track responses. Even if one can simulate the same response to sea ice loss using different methods it is still important to understand the underlying mechanism. It is unclear what mechanism underlies the imposed ghost forcing in the ice module. Future work should focus on better understanding how each method of imposing sea ice loss impacts the energetics of the atmospheric and oceanic response to sea ice loss, particularly in the Arctic Ocean (Timmermans et al. 2018; Timmermans and Marshall 2020).

Previous work by Kim et al. (2018) showed there was no significant annual-mean polar amplification of surface temperature in response to doubled CO_2 in an aquaplanet with a seasonal cycle and no sea ice. Consistently our aquaplanet simulations with a seasonal cycle show that in response to quadrupled CO_2 annual-mean polar amplification emerges only with climatological sea ice. Furthermore, our aquaplanet results show that significant latent energy transport into the polar region is not a necessary or sufficient condition for polar amplification. Finally, the importance of sea ice for polar amplification is consistent with recent work that highlighted the annual-mean near-surface climatological inversion in the polar region only occurs in the presence of sea ice (Miyawaki et al. 2022) and that sea ice melting and Arctic amplification are connected in reanalysis data and coupled climate models (Screen and Simmonds 2010; Dai et al. 2020; Feldl et al. 2020). Since sea ice loss due to melting can be constrained by sea ice albedo using modern satellite and reanalysis data (Thackeray and Hall 2019), future work will focus on leveraging the connection between sea ice and the midlatitude atmosphere.

Acknowledgments. TAS and ZS acknowledge support from NSF (AGS-1742944 and AGS-2033467). The authors thank M. England for providing the WACCM data and S. Hay and P. Kushner for providing the CESM data. The authors also thank three anonymous reviewers for their comments, which

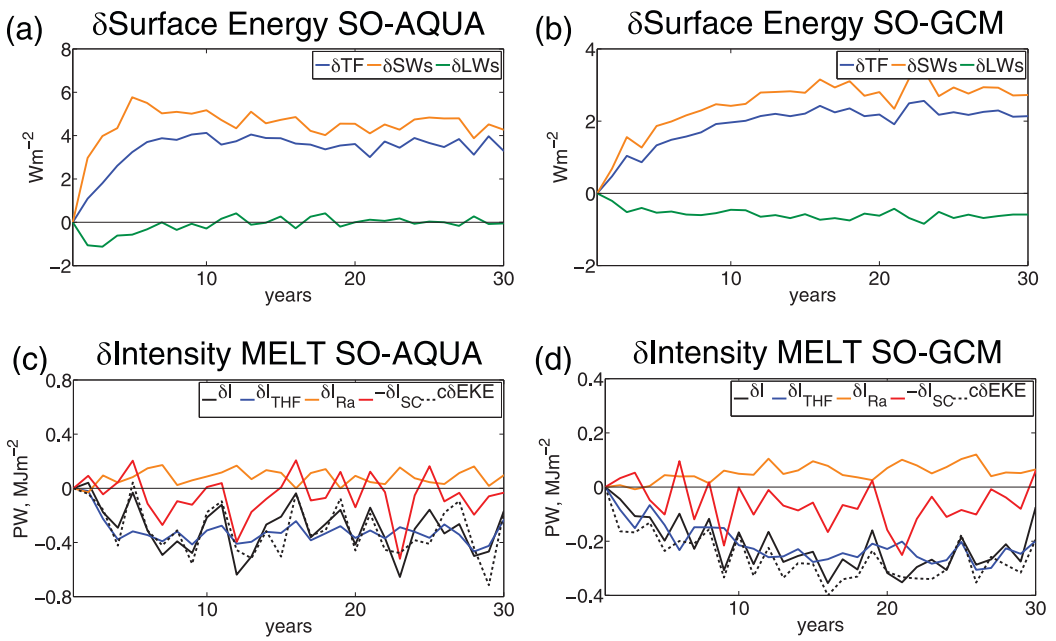

FIG. 14. Transient response of annual-mean, zonally averaged flux form (each term has the global mean removed) (a),(b) surface energy budget in the polar region and (c),(d) midlatitude storm-track intensity response to sea ice loss due to melting for (a),(c) SO-AQUA and (b),(d) SO-GCM. The intensity response is decomposed into contributions from surface turbulent fluxes (δI_{TF}), radiative cooling (δI_{Ra}), and stationary circulation ($-\delta I_{\mathrm{SC}}$).

significantly improved the manuscript. The ECHAM6 aquaplanet and atmospheric general circulation model simulations in this paper were completed with resources provided by the University of Chicago Research Computing Center.

Data availability statement. Data supporting this study are available through Knowledge@UChicago (https://doi.org/10.6082/uchicago.2933).

REFERENCES

Audette, A., and Coauthors, 2021: Opposite responses of the dry and moist eddy heat transport into the Arctic in the PAMIP experiments. *Geophys. Res. Lett.*, **48**, e2020GL089990, https://doi.org/10.1029/2020GL089990.

Barnes, E. A., 2013: Revisiting the evidence linking Arctic amplification to extreme weather in midlatitudes. *Geophys. Res. Lett.*, **40**, 4734–4739, https://doi.org/10.1002/grl.50880.

——, and J. A. Screen, 2015: The impact of Arctic warming on the midlatitude jet-stream: Can it? Has it? Will it? *Wiley Interdiscip. Rev.: Climate Change*, **6**, 277–286, https://doi.org/10.1002/wcc.337.

Barpanda, P., and T. A. Shaw, 2017: Using the moist static energy budget to understand storm-track shifts across a range of time scales. *J. Atmos. Sci.*, **74**, 2427–2446, https://doi.org/10.1175/JAS-D-17-0022.1.

——, and ——, 2020: Surface fluxes modulate the seasonality of zonal-mean storm tracks. *J. Atmos. Sci.*, **77**, 753–779, https://doi.org/10.1175/JAS-D-19-0139.1.

Blackport, R., and P. Kushner, 2016: The transient and equilibrium climate response to rapid summertime sea ice loss in CCSM4. *J. Climate*, **29**, 401–417, https://doi.org/10.1175/JCLI-D-15-0284.1.

——, and ——, 2017: Isolating the atmospheric circulation response to Arctic sea ice loss in the coupled climate system. *J. Climate*, **30**, 2163–2185, https://doi.org/10.1175/JCLI-D-16-0257.1.

——, and J. A. Screen, 2020: Weakened evidence for mid-latitude impacts of Arctic warming. *Nat. Climate Change*, **10**, 1065–1066, https://doi.org/10.1038/s41558-020-00954-y.

Butler, A. H., D. W. J. Thompson, and R. Heikes, 2010: The steady-state atmospheric circulation response to climate change–like thermal forcings in a simple general circulation model. *J. Climate*, **23**, 3474–3496, https://doi.org/10.1175/2010JCLI3228.1.

Cohen, J., and Coauthors, 2014: Recent Arctic amplification and extreme mid-latitude weather. *Nat. Geosci.*, **7**, 627–637, https://doi.org/10.1038/ngeo2234.

——, and Coauthors, 2020: Divergent consensuses on Arctic amplification influence on midlatitude severe winter weather. *Nat. Climate Change*, **10**, 20–29, https://doi.org/10.1038/s41558-019-0662-y.

Dai, A., D. Luo, M. Son, and J. Liu, 2020: Arctic amplification is caused by sea-ice loss under increasing CO_2. *Nat. Commun.*, 10, 121, https://doi.org/10.1038/s41467-018-07954-9.

Deser, C., R. A. Tomas, and L. Sun, 2015: The role of ocean–atmosphere coupling in the zonal mean atmospheric response to Arctic sea ice loss. *J. Climate*, **28**, 2168–2186, https://doi.org/10.1175/JCLI-D-14-00325.1.

——, L. Sun, R. A. Tomas, and J. Screen, 2016: Does ocean coupling matter for the northern extratropical response to projected Arctic sea ice loss? *Geophys. Res. Lett.*, **43**, 2149–2157, https://doi.org/10.1002/2016GL067792.

Donohoe, A., and D. S. Battisti, 2012: What determines the meridional heat transport in climate models? *J. Climate*, **25**, 3832–3850, https://doi.org/10.1175/JCLI-D-11-00257.1.

England, M., L. M. Polvani, and L. Sun, 2018: Contrasting the Antarctic and Arctic atmospheric responses to projected sea ice loss in the late twenty-first century. *J. Climate*, **31**, 6353–6370, https://doi.org/10.1175/JCLI-D-17-0666.1.

——, ——, ——, and C. Deser, 2020: Tropical climate responses to projected Arctic and Antarctic sea-ice loss. *Nat. Geosci.*, **13**, 275–281, https://doi.org/10.1038/s41561-020-0546-9.

Feldl, N., S. Po-Chedley, H. K. A. Singh, S. Hay, and P. J. Kushner, 2020: Sea ice and atmospheric circulation shape the high-latitude lapse rate feedback. *npj Climate Atmos. Sci.*, **3**, 41, https://doi.org/10.1038/s41612-020-00146-7.

Francis, J., 2017: Why are Arctic linkages to extreme weather still up in the air? *Bull. Amer. Meteor. Soc.*, **98**, 2551–2557, https://doi.org/10.1175/BAMS-D-17-0006.1.

Giorgetta, M. A., and Coauthors, 2013: The atmospheric general circulation model ECHAM6: Model description. Reports on Earth System Science, 177 pp., https://www.cen.uni-hamburg.de/en/icdc/data/atmosphere/docs-atmo/echam6-scidoc.pdf.

Graversen, R. G., T. Mauritsen, M. Tjernstrom, E. Kallen, and G. Svensson, 2008: Vertical structure of recent Arctic warming. *Nature*, **451**, 53–56, https://doi.org/10.1038/nature06502.

Harvey, B. J., L. C. Shaffrey, and T. J. Woollings, 2014: Equator-to-pole temperature differences and the extra-tropical storm-track responses of the CMIP5 climate models. *Climate Dyn.*, **43**, 1171–1182, https://doi.org/10.1007/s00382-013-1883-9.

——, ——, and ——, 2015: Deconstructing the climate change response of the Northern Hemisphere wintertime storm tracks. *Climate Dyn.*, **45**, 2847–2860, https://doi.org/10.1007/s00382-015-2510-8.

Held, I., 2005: The gap between simulation and understanding in climate modeling. *Bull. Amer. Meteor. Soc.*, **86**, 1609–1614, https://doi.org/10.1175/BAMS-86-11-1609.

Hell, M., T. Schneider, and C. Li, 2020: Atmospheric circulation response to short-term Arctic warming in an idealized model. *J. Atmos. Sci.*, **77**, 531–549, https://doi.org/10.1175/JAS-D-19-0133.1.

Hwang, Y.-T., and D. Frierson, 2010: Increasing atmospheric poleward energy transport with global warming. *Geophys. Res. Lett.*, **37**, L24807, https://doi.org/10.1029/2010GL045440.

Kang, S. M., I. M. Held, D. M. W. Frierson, and M. Zhao, 2008: The response of the ITCZ to extratropical thermal forcing: Idealized slab-ocean experiments with a GCM. *J. Climate*, **21**, 3521–3532, https://doi.org/10.1175/2007JCLI2146.1.

Kay, J. E., M. M. Holland, C. M. Bitz, E. Blanchard-Wrigglesworth, A. Gettleman, A. Conley, and D. Bailey, 2012: The influence of local feedbacks and northward heat transport on the equilibrium Arctic climate response to increased greenhouse gas forcing. *J. Climate*, **25**, 5433–5450, https://doi.org/10.1175/JCLI-D-11-00622.1.

Kim, D., S. M. Kang, Y. Shin, and N. Feldl, 2018: Sensitivity of polar amplification to varying insolation conditions. *J. Climate*, **31**, 4933–4947, https://doi.org/10.1175/JCLI-D-17-0627.1.

Labe, Z. M., Y. Peings, and G. Magnusdottir, 2020: Warm Arctic, cold Siberia pattern: Role of full Arctic amplification versus sea ice loss alone. *Geophys. Res. Lett.*, **47**, e2020GL088583, https://doi.org/10.1029/2020GL088583.

Maher, P., and Coauthors, 2019: Model hierarchies for understanding atmospheric circulation. *Rev. Geophys.*, **57**, 250–280, https://doi.org/10.1029/2018RG000607.

Manabe, S., and R. T. Wetherald, 1975: The effects of doubling the CO_2 concentration on the climate of a general circulation model. *J. Atmos. Sci.*, **32**, 3–15, https://doi.org/10.1175/1520-0469(1975)032<0003:TEODTC>2.0.CO;2.

McCusker, K. E., J. C. Fyfe, and M. Sigmond, 2016: Twenty-five winters of unexpected Eurasian cooling unlikely due to Arctic sea-ice loss. *Nat. Geosci.*, **9**, 838–842, https://doi.org/10.1038/ngeo2820.

——, P. J. Kushner, F. C. Fyfe, M. Sigmond, V. V. Kharin, and C. M. Bitz, 2017: Remarkable separability of circulation response to Arctic sea ice loss and greenhouse gas forcing. *Geophys. Res. Lett.*, **44**, 7955–7964, https://doi.org/10.1002/2017GL074327.

McGraw, M. C., and E. A. Barnes, 2016: Seasonal sensitivity of the eddy-driven jet to tropospheric heating in an idealized AGCM. *J. Climate*, **29**, 5223–5240, https://doi.org/10.1175/JCLI-D-15-0723.1.

Merlis, T. M., and M. Henry, 2018: Simple estimates of polar amplification in moist diffusive energy balance models. *J. Climate*, **31**, 5811–5824, https://doi.org/10.1175/JCLI-D-17-0578.1.

Miyawaki, O., T. A. Shaw, and M. F. Jansen, 2022: Quantifying energy balance regimes in the modern climate, their link to lapse rate regimes, and their response to warming. *J. Climate*, **35**, 1045–1061, https://doi.org/10.1175/JCLI-D-21-0440.1.

O'Gorman, P. A., and T. Schneider, 2008: Energy of midlatitude transient eddies in idealized simulations of changed climates. *J. Climate*, **21**, 5797–5806, https://doi.org/10.1175/2008JCLI2099.1.

Oudar, T., E. Sanchez-Gomez, F. Chauvin, J. Cattiaux, L. Terray, and C. Cassou, 2017: Respective roles of direct GHG radiative forcing and induced Arctic sea ice loss on the Northern Hemisphere atmospheric circulation. *Climate Dyn.*, **49**, 3693–3713, https://doi.org/10.1007/s00382-017-3541-0.

Overland, J., J. A. Francis, R. Hall, E. Hanna, S.-J. Kim, and T. Vihma, 2015: The melting Arctic and midlatitude weather patterns: Are they connected? *J. Climate*, **28**, 7917–7932, https://doi.org/10.1175/JCLI-D-14-00822.1.

Polvani, L. M., A. C. Clement, B. Medeiros, J. J. Benedict, and I. R. Simpson, 2017: When less is more: Opening the door to simpler climate models. *Eos*, **98**, https://doi.org/10.1029/2017EO079417.

Ronalds, B., and E. A. Barnes, 2019: A role for barotropic eddy-mean flow feedbacks in the zonal wind response to sea ice loss and Arctic amplification. *J. Climate*, **32**, 7469–7481, https://doi.org/10.1175/JCLI-D-19-0157.1.

Screen, J. A., and I. Simmonds, 2010: The central role of diminishing sea ice in recent Arctic temperature amplification. *Nature*, **464**, 1334–1337, https://doi.org/10.1038/nature09051.

——, and Coauthors, 2018: Consistency and discrepancy in the atmospheric response to Arctic sea-ice loss across climate models. *Nat. Geosci.*, **11**, 155–163, https://doi.org/10.1038/s41561-018-0059-y.

Shaw, T. A., 2019: Mechanisms of future predicted changes in the zonal mean mid-latitude circulation. *Curr. Climate Change Rep.*, **5**, 345–357, https://doi.org/10.1007/s40641-019-00145-8.

——, and R. J. Graham, 2020: Hydrological cycle changes explain weak snow ball Earth storm track despite increased surface baroclinicity. *Geophys. Res. Lett.*, **47**, e2020GL089866, https://doi.org/10.1029/2020GL089866.

——, and Coauthors, 2016: Storm track processes and the opposing influences of climate change. *Nat. Geosci.*, **9**, 656–664, https://doi.org/10.1038/ngeo2783.

——, P. Barpanda, and A. Donohoe, 2018: A moist static energy framework for zonal-mean storm-track intensity. *J. Atmos. Sci.*, **75**, 1979–1994, https://doi.org/10.1175/JAS-D-17-0183.1.

Smith, D. M., and Coauthors, 2019: The Polar Amplification Model Intercomparison Project (PAMIP) contribution to CMIP6: Investigating the causes and consequences of polar amplification. *Geosci. Model Dev.*, **12**, 1139–1164, https://doi.org/10.5194/gmd-12-1139-2019.

Stevens, B., M. Giorgetta, M. Esch, T. Mauritsen, T. Crueger, and S. Rast, 2013: Atmospheric component of the MPI-M Earth system model: ECHAM6. *J. Adv. Model. Earth Syst.*, **5**, 146–172, https://doi.org/10.1002/jame.20015.

Sun, L., M. Alexander, and C. Deser, 2018: Evolution of the global coupled climate response to Arctic sea ice loss during 1990–2090 and its contribution to climate change. *J. Climate*, **31**, 7823–7843, https://doi.org/10.1175/JCLI-D-18-0134.1.

——, C. Deser, R. A. Tomas, and M. Alexander, 2020: Global coupled climate response to polar sea ice loss: Evaluating the effectiveness of different ice-constraining approaches. *Geophys. Res. Lett.*, **47**, e2019GL085788, https://doi.org/10.1029/2019GL085788.

Thackeray, C. W., and A. Hall, 2019: An emergent constraint on future Arctic sea-ice albedo feedback. *Nat. Climate Change*, **9**, 972–978, https://doi.org/10.1038/s41558-019-0619-1.

Timmermans, M.-L., and J. Marshall, 2020: Understanding Arctic Ocean circulation: A review of ocean dynamics in a changing climate. *J. Geophys. Res. Oceans*, **125**, e2018JC014378, https://doi.org/10.1029/2018JC014378.

——, J. Toole, and R. Krishfield, 2018: Warming of the interior Arctic Ocean linked to sea ice losses at the basin margins. *Sci. Adv.*, **4**, eaat6773, https://doi.org/10.1126/sciadv.aat6773.

Tomas, R., C. Deser, and L. Sun, 2016: The role of ocean heat transport in the global climate response to projected Arctic sea ice loss. *J. Climate*, **29**, 6841–6859, https://doi.org/10.1175/JCLI-D-15-0651.1.

Wang, K., C. Deser, L. Sun, and R. A. Tomas, 2018: Fast response of the tropics to an abrupt loss of Arctic sea ice via ocean dynamics. *Geophys. Res. Lett.*, **45**, 4264–4272, https://doi.org/10.1029/2018GL077325.

Wu, Y., and K. L. Smith, 2016: Response of Northern Hemisphere midlatitude circulation to Arctic amplification in a simple atmospheric general circulation model. *J. Climate*, **29**, 2041–2058, https://doi.org/10.1175/JCLI-D-15-0602.1.

Yuval, J., and Y. Kaspi, 2020: Eddy activity response to global warming-like temperature changes. *J. Climate*, **33**, 1381–1404, https://doi.org/10.1175/JCLI-D-19-0190.1.